Title

Effects of temperature and gas—liquid mass transfer on the operation of small electrochemical cells for the quantitative evaluation of CO 2 reduction electrocatalysts

Journal

Physical Chemistry Chemical Physics, 18(38)

ISSN

1463-9076

Authors

Lobaccaro, Peter

Singh, Meenesh R

Clark, Ezra Lee

et al.

Publication Date

2016-09-29

DOI

10.1039/c6cp05287h

Peer reviewed

PCCP

PAPER

View Article Online
View Journal

Cite this: DOI: 10.1039/c6cp05287h

Effects of temperature and gas–liquid mass transfer on the operation of small electrochemical cells for the quantitative evaluation of CO_2 reduction electrocatalysts†

Peter Lobaccaro,[abc] Meenesh R. Singh,[abc] Ezra Lee Clark,[abc] Youngkook Kwon,[ab] Alexis T. Bell*[abc] and Joel W. Ager*[ade]

In the last few years, there has been increased interest in electrochemical CO_2 reduction (CO2R). Many experimental studies employ a membrane separated, electrochemical cell with a mini H-cell geometry to characterize CO2R catalysts in aqueous solution. This type of electrochemical cell is a mini-chemical reactor and it is important to monitor the reaction conditions within the reactor to ensure that they are constant throughout the study. We show that operating cells with high catalyst surface area to electrolyte volume ratios (*S*/*V*) at high current densities can have subtle consequences due to the complexity of the physical phenomena taking place on electrode surfaces during CO2R, particularly as they relate to the cell temperature and bulk electrolyte CO_2 concentration. Both effects were evaluated quantitatively in high *S*/*V* cells using Cu electrodes and a bicarbonate buffer electrolyte. Electrolyte temperature is a function of the current/total voltage passed through the cell and the cell geometry. Even at a very high current density, 20 mA cm^{-2}, the temperature increase was less than 4 °C and a decrease of <10% in the dissolved CO_2 concentration is predicted. In contrast, limits on the CO_2 gas–liquid mass transfer into the cells produce much larger effects. By using the pH in the cell to measure the CO_2 concentration, significant undersaturation of CO_2 is observed in the bulk electrolyte, even at more modest current densities of 10 mA cm^{-2}. Undersaturation of CO_2 produces large changes in the faradaic efficiency observed on Cu electrodes, with H_2 production becoming increasingly favored. We show that the size of the CO_2 bubbles being introduced into the cell is critical for maintaining the equilibrium CO_2 concentration in the electrolyte, and we have designed a high *S*/*V* cell that is able to maintain the near-equilibrium CO_2 concentration at current densities up to 15 mA cm^{-2}.

Received 30th July 2016,
Accepted 6th September 2016

DOI: 10.1039/c6cp05287h

www.rsc.org/pccp

Introduction

Conversion of atmospheric CO_2 to fuels and value-added chemicals is a potential approach to combat the emission of greenhouse gases and, eventually, allow for a closed-loop global carbon cycle.[1–3] Electrochemical reduction of CO_2 (CO2R) has been proposed as one possible technology for the production of fuels from CO_2 using electricity obtained from renewable sources.[4–7] Studies of CO2R in aqueous solution date back to the 1950s,[8] and an extensive and thorough body of work was published by Hori and co-workers starting in the 1980s.[9–14] This work identified the key challenges in implementing electrochemical CO2R for fuel or chemical synthesis. While there are metal catalysts that show high degrees of selectivity to carbon monoxide (*e.g.* Ag and Au) or formic acid (*e.g.* Pb, In, and Sn), copper is the only known metal that shows activity to producing more reduced hydrocarbons and alcohols at appreciable current densities (~10 mA cm^{-2}). Recently, there has been a renewal of interest in electrochemical CO2R, with reports of both reductions in overpotentials for 2 electron products such as CO[15] and formate[16] and improved selectivity for higher order products such as ethylene[17] and ethanol.[18] However, there are still no known catalysts which show high selectivity to a

[a] Joint Center for Artificial Photosynthesis, Lawrence Berkeley National Laboratory, CA 94720, USA. E-mail: alexbell@berkeley.edu, jwager@lbl.gov
[b] Chemical Sciences Division, Lawrence Berkeley National Laboratory, CA 94720, USA
[c] Department of Chemical and Biomolecular Engineering, University of California, Berkeley, CA 94720, USA
[d] Materials Sciences Division, Lawrence Berkeley National Laboratory, CA 94720, USA
[e] Department of Materials Science and Engineering, University of California, Berkeley, CA 94720, USA

† Electronic supplementary information (ESI) available. See DOI: 10.1039/c6cp05287h

CO2R product requiring more than 2 electron transfers. Clearly, improvements in both CO2R catalyst activity and selectivity will be required if there is to be widespread implementation of this technology.[19–22]

In order to drive progress in the CO2R electrocatalysis community, commonly accepted, easily reproducible testing conditions need to be established,[23] similar to those suggested for photoelectrochemical water splitting.[24] Hori and co-workers have already identified many good practices for experimentation in this area[10,13,25,26] and some further insight into polarization losses was provided by Singh *et al.*[27] However, examining the recent literature, one can observe that several different methods of analyzing CO2R electrocatalysts have been used which employ different cell designs and testing conditions.

In particular, the cell designs vary widely (see ESI† for a detailed comparison). In many designs, CO_2[13,18,28–34] or the electrolyte[35] (or both[36,37]) is flowed through the cell; in others, the cell is charged initially and then sealed.[15] Reactor vessels range from classic Pyrex H-cells[10,28,32,34] to compact sandwich compression cells.[29–31,36,37] The electrochemical cells used for the analysis of CO2R catalysts are, in fact, miniature chemical reactors in which known reaction conditions must be maintained.[38] This concept has been emphasized in the electrochemical engineering literature,[39–41] with a number of studies focused on gas sparged systems[42–45] similar in design to the cells described above. Notably, the dilute electrolyte conditions and corresponding mass transfer limitations typical of CO2R make the cell design implications even more important.

The compact sandwich compression cells are of particular interest. This design can reduce the electrolyte volume (V) compared to the electrode surface area (S), allowing liquid products to accumulate in the uncirculated electrolyte to a detectable level more quickly. Notably, the use of this type of high S/V (>0.5 cm^{-1}) cell led to insights into the CO2R mechanism on copper through the detection of five previously unreported trace liquid products.[31] However, when using high S/V cells there could be an increased potential for heating to occur in the cell due to the lower thermal mass of electrolyte and for dissolved CO_2 in the electrolyte to be depleted.[39,46] It is known that the cell temperature can change catalyst activity, in part due to the change in CO_2 solubility.[10] Furthermore, maintaining CO_2 saturation in general may be difficult due to the slow dissolution kinetics of CO_2 in water, as has been recently experimentally quantified for a system similar to that used in CO2R.[47] In either case the concern arises that deviations from expected standard testing conditions could occur which would cause the catalytic activity measurement to incorrectly reflect the true catalytic activity of a material.

Here we critically examine the near-equilibrium steady-state operation of high S/V, sandwich type, electrochemical cells for CO2R catalyst characterization. We illustrate how changes in the electrolyte temperature and in the dissolved CO_2 concentration can affect the electrolyte composition and electrolyte pH. Importantly, we show that changes in gas–liquid mass transfer within the cell can cause CO_2 depletion in the bulk electrolyte and that this has a pronounced effect on the observed product distribution for Cu electrodes. Finally, we outline the design parameters required to operate high S/V electrochemical cells under near equilibrium, steady-state conditions, providing guidance towards standardizing electrochemical CO2R catalyst characterization conditions.

Experimental

Electrochemical cell design

An overview of the cell design will be given here; a full description of the cell design can be found in the ESI.† Two compression-sealed electrochemical cells with the same overall architecture were constructed for the study. Both cells have a cathode surface area of 1 cm^2. The primary difference between the cells is the volume of electrolyte in the cathode and anode chambers: 0.5 cm^3 for cell A (Fig. S1, ESI†) *versus* 1.5 cm^3 for cell B (Fig. 1), yielding S/V ratios of 2 cm^{-1} and 0.67 cm^{-1}, respectively. We emphasize that a larger S/V ratio should lead to faster liquid product accumulation and thus shorter run times and more sensitive product detection (see ESI† for detailed discussion). Cell A was designed to create the maximum S/V ratio possible with a typical 1 cm^2 cathode while still incorporating replaceable CO_2 bubblers and gas tight fittings. Cell B was the highest S/V design possible in which a removable glass frit bubbler could be installed to reduce the size of the sparging CO_2 bubbles, an effect we will later show is important.

The cells are composed of an anode and cathode chamber, separated by an anion-conducting membrane, Selemion AMV (AGC Engineering Co.). The two chambers were fabricated from polycarbonate, and all components were designed to be removable for cleaning purposes. It is advantageous to have a cell with replaceable parts since small contamination sources can have a disproportionally large effect on the results of CO2R studies.[25,48] The cell was also designed to maintain parallel plate electrode geometry to ensure a uniform voltage field over the catalyst surface.

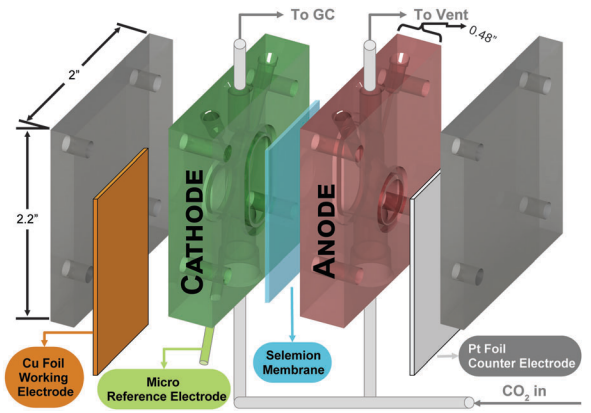

Fig. 1 CO2R electrochemical cell design: cell B with the larger electrolyte volume is pictured here, a schematic of cell A is shown in Fig. S1 (ESI†). The cell is made up of two polycarbonate compartments with identical volumes separated by a membrane. Both sides are sparged with CO_2 and the gaseous products produced at the cathode are swept away to be analyzed by GC. The liquid products in the cathode chamber accumulate over the course of the reaction and are analyzed by HPLC.

A 1 mm OD Ag/AgCl reference electrode (Innovative Instruments) was inserted into the cathode chamber to monitor the working electrode potential. This reference electrode was calibrated against an ideal reversible hydrogen electrode. The cell was sealed by compressing the stack of counter electrode, anode chamber, membrane, cathode chamber, and working electrode between two outer plates secured with bolts. The seals were made with Buna-N O-rings (Apple Rubber). During measurements, both sides of the cell were sparged with CO_2 at 1 atmosphere and the gas exiting the cathode compartment was directed to a gas chromatograph (GC) for gaseous product analysis.

Electrochemical cell operation

99.9999% base metal pure sodium carbonate (Na_2CO_3) (Sigma-Aldrich) was used as the precursor salt for making the 0.1 M sodium bicarbonate ($NaHCO_3$) electrolyte used in this study. The conversion of carbonate to bicarbonate electrolyte is achieved by sparging the carbonate electrolyte with 1 atmosphere of CO_2. All water used in these experiments was provided by a Millipore water system producing 18.2 MΩ cm resistivity water with less than 5 ppb total organic carbon concentration. 99.9999% 0.1 mm thick copper (Cu) foil (Alfa-Aesar) was used for the working electrode. The foil was cut into 2 × 2 cm pieces and degreased by sonication in acetone and iso-propyl alcohol for 60 minutes each. Before use, each foil was electrochemically polished. ACS grade phosphoric acid (Sigma-Aldrich) was used as the bath (~300 mL) and the bath was stirred with a Teflon stir bar at ~400 rpm. A 99.9999% pure 0.1 mm thick Cu foil was used as the counter electrode. The electrodes were set 20 mm apart and then polished at +2 V *vs.* the counter electrode for 5 minutes with a Biologic VSP-200 potentiostat.

The cell was assembled with a new electropolished Cu foil working electrode, a platinum foil counter electrode, and a piece of Selemion membrane. Before each experiment 0.5 mL or 1.5 mL of electrolyte was injected into each compartment of cell A and cell B, respectively, and CO_2 was bubbled through the cell. A Biologic VSP-300 potentiostat with electrochemical impedance package was used throughout the remaining experiments and was first used to measure the electrochemical impedance of the cell in order to enable *in situ* ohmic resistance correction. 75% compensation was used to correct for the cell resistance (the uncompensated resistance was ~40 Ohms for cell A and ~80 Ohms for cell B). A constant voltage was applied *versus* the Ag/AgCl reference electrode for 2 hours and the product distribution measured by the GC was converted back into faradaic efficiencies for each product. Additional details of this experimental process can be found in the ESI.†

Gaseous product detection

The methods for detecting the products of CO2R are well established.[13,49] Here, the CO_2 flow through the cell sweeps away the gaseous products evolving at the cathode. The CO_2 stream exiting the cell was passed through the sampling loop of a GC which can identify the expected gaseous reaction products, namely hydrogen (H_2), carbon monoxide (CO), methane (CH_4), and ethylene (C_2H_4).

The CO_2 flow rate was set with some care. It must be high enough to provide good mixing in the chamber as well as to maintain the saturation of CO_2 in the electrolyte. On the other hand, higher flow rates can dilute the concentration of gaseous products below the quantitative detection range of the analytical equipment. Based on these considerations, the flow rate of CO_2 through both the cathode and anode chambers was set to 5 sccm throughout all experiments. For the GC used here (SRI multigas #3 GC), the quantitative detection limits are ~100 ppm for H_2 and ~2 ppm for CO, CH_4, and C_2H_4. At the chosen flow rate and a cathode area of 1 cm^2, the minimum detectable partial current densities are 1.5 μA cm^{-2} (CO), 5 μA cm^{-2} (CH_4), 8 μA cm^{-2} (C_2H_4), and 70 μA cm^{-2} (H_2). Ethane (C_2H_6) can also be detected with our GC method but was not observed in any experiments performed in this study. Gas from the cell was sampled every 20 minutes, corresponding to the cycle time of the GC analysis. We note that the CO_2 flow through the cell could potentially entrain volatile liquid products; however, this can generally be mitigated by hydrating the CO_2 before it enters the cell. Additional details about product detection are in the ESI.†

Liquid product detection

Liquid products evolved at the cathode mix with the electrolyte in the cell and must accumulate for a sufficient period of time in order to reach the detection limits of typical analytical tools, such as nuclear magnetic resonance (NMR) or high pressure liquid chromatography (HPLC). Liquid products were detected by HPLC at the end of the run (2 hours) by extracting the electrolyte from both the anode and cathode chamber. Analysis of both chambers is required as negatively charged species evolved at the cathode, such as formate and acetate, can cross the anion conducting membrane and accumulate in the anode chamber. As discussed in the ESI,† for a run with similar electrochemical parameters, the concentration of liquid products in cell A, with a larger S/V ratio, was larger than that produced by cell B, as expected.

Electrolyte temperature measurements

To evaluate cell heating during operation, the cell was assembled exactly as it was for the product analysis experiments, except the cell was not connected to the GC. A 0.5 mm OD stainless steel thermocouple (omega) was inserted to monitor the electrolyte temperature in each chamber of the electrochemical cell every 5 minutes. The small size of the thermocouple ensured a very small thermal load on the system so as not to influence the temperature in the small amount of electrolyte. The thermocouple was also not left in the solution for more than the 10 seconds required to get an accurate reading. The temperature was recorded at each current density over a 1 hour period to ensure a steady-state temperature was reached.

Electrolyte pH measurements

The cell was assembled exactly as it was for the product analysis experiments, except the cell was not connected to the GC. Two different pH probes were used to acquire *in situ* measurements in the two cells. A 1 mm OD pH probe (Innovative Instruments)

was used to measure the pH in cell A, the small diameter being required for a cell of that size. A Hanna Instruments pH probe, ~3 mm in diameter, was used to measure the pH in cell B. Both probes were calibrated with 7.01 and 4.01 buffer standards (Hanna Instruments) before each measurement. The measurement uncertainty of the small probe was larger than that of the larger Hanna probe; this is reflected in the error bars in the figures.

In order to get a pH measurement that accurately reflected the pH of the electrolyte during experimentation, the experiment was precisely halted by stopping the bubbling and potential applied to the cell at the same time. The respective pH probes where then carefully inserted into both chambers of the cell to obtain a reading. The anode chamber, which was being constantly sparged with CO_2 but did not consume CO_2, provided an internal reference point to ensure that the pH probes were taking accurate measurements. The pH of each chamber was measured before and after 1 hour of electrocatalysis over a range of current densities.

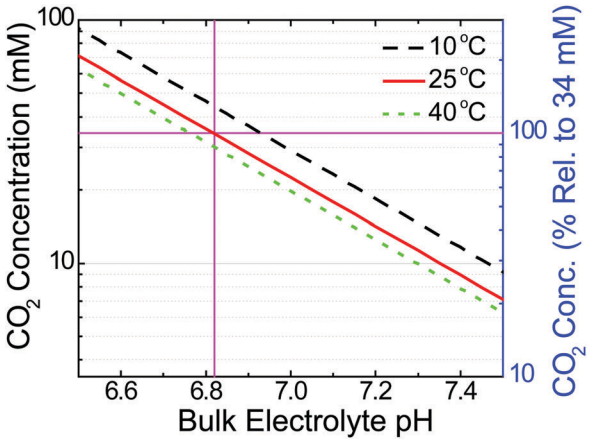

Fig. 2 CO_2 Concentration *vs.* pH: by solving eqn (1)–(5), the equilibrium relationship between dissolved CO_2 concentration and pH was obtained for a 0.1 M $NaHCO_3$ electrolyte by varying the gas phase pressure of CO_2. The pink lines indicate the equilibrium CO_2 concentration (34.2 mM) at 25 °C and 1 atmosphere of CO_2; the right hand axis is normalized to this value.

Results and discussion

CO_2/carbonate family thermodynamic relations

The relevant chemical equilibria for the CO_2, bicarbonate, carbonate family in aqueous solution are:

$$CO_{2(g)} \rightleftharpoons CO_{2(aq)} \quad (1)$$

$$CO_{2(aq)} + H_2O \rightleftharpoons H^+ + HCO_3^- \quad (2)$$

$$HCO_3^- \rightleftharpoons H^+ + CO_3^{2-} \quad (3)$$

$$H_2O \rightleftharpoons H^+ + OH^- \quad (4)$$

with corresponding equilibrium constants: K_0 (Henry's law constant), K_1, K_2, and K_w. The term for $CO_{2(aq)}$ includes both dissolved CO_2 and the very small amount of carbonic acid which would be expected under these conditions.[47] Additionally, charge neutrality within the electrolyte must be maintained, shown here for a $NaHCO_3$ solution:

$$[HCO_3^-] + 2[CO_3^{2-}] + [OH^-] = [Na^+] + [H^+] \quad (5)$$

The thermodynamics of CO_2 in water[50–53] and salt solutions[54–60] has been widely studied since the 19th century. The value of K_0 depends on the electrolyte and generally decreases with increasing ionic strength, leading to the "salting-out" effect.[60–62] However, at the ionic strength used here, 0.1 M, the CO_2 solubility would be expected to be reduced by less than 5% (see ESI† for details).[62] Salt concentration is also known to affect the acid dissociation constants.[57–59] However, again, these changes are predicted to be small for the conditions employed here. Thus, for this study the equilibrium thermodynamic relations for the carbonate system were taken from those recommended for pure water.[53,63]

From eqn (1)–(5), it is clear that if the salt concentration, solution temperature, and CO_2 pressure in the headspace are known, then the solution pH can be calculated. For a 0.1 M $NaHCO_3$ solution at 25 °C, the solution pH should be 6.82 with a dissolved CO_2 concentration of 34.2 mM.[60] We were able to confirm this calculation by measuring a pH of 6.82 ± 0.01 for a 0.1 M $NaHCO_3$ solution which was allowed to equilibrate with 1 atm of CO_2 at 25 °C. Experimentally, it is convenient to make a temperature corrected pH measurement, whereas measuring the dissolved CO_2 concentration is not as readily accessible.[47,51,60] Using the thermodynamic relationships established above, pH and temperature can be readily used to calculate the CO_2 concentration in an electrolyte of known concentration, as shown in Fig. 2 for three temperatures. Interestingly, under the driving conditions of CO_2 bubbling typically used in our experiments, a lower pH of ~6.7 was typically observed. This lower pH is due to a supersaturated concentration of dissolved CO_2 in the electrolyte; this is a frequently observed phenomena.[64,65]

Effect of *in situ* heating

In situ heating of the cell could be expected due to the overpotentials required to drive the reaction at both the cathode and anode and due to the ohmic and polarization losses caused by the finite conductivity of the electrolyte and the transport limitations of the ionic species. As most CO2R catalysts require very large overpotentials (greater than 1 V) to drive appreciable CO2R currents,[21] the heating of the cell could be appreciable. As the temperature in the cell rises, the CO_2 solubility in the electrolyte will decrease, which could affect the observed kinetics and selectivity of the reaction. Fig. 3, which was obtained by solving eqn (1)–(5) for a 0.1 M $NaHCO_3$ buffer solution at 1 atm of CO_2, illustrates the effect of temperature on solution pH and dissolved CO_2 concentration. It can be seen that the temperature slightly changes the bulk electrolyte pH and for only a 5 °C shift in electrolyte temperature the concentration of dissolved CO_2 changes by more than 10%.

To assess the importance of cell heating, the temperature in cell A and cell B was measured as a function of current density from 7.5 to 20 mA cm^{-2} (Fig. 4). In both cells the change in electrolyte temperature was small, less than 2 °C up to 15 mA cm^{-2},

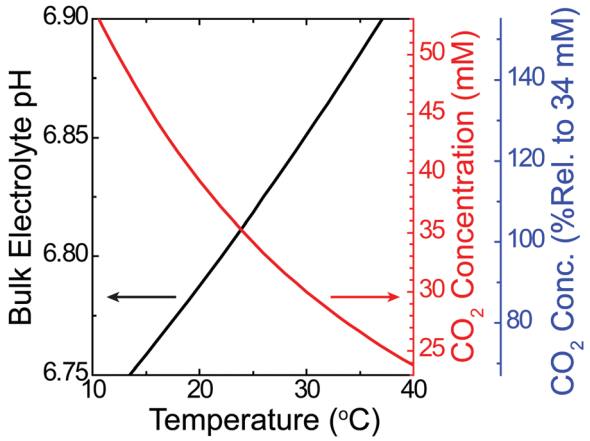

Fig. 3 Temperature effect on electrolyte: by solving eqn (1)–(5), the effect of temperature on the equilibrium pH (black) and equilibrium dissolved CO_2 concentration (red) was obtained for a 0.1 M $NaHCO_3$ electrolyte in equilibrium with 1 atm of CO_2. The far right hand axis (blue) shows the dissolved CO_2 concentration normalized to the value for 25 °C (34.2 mM).

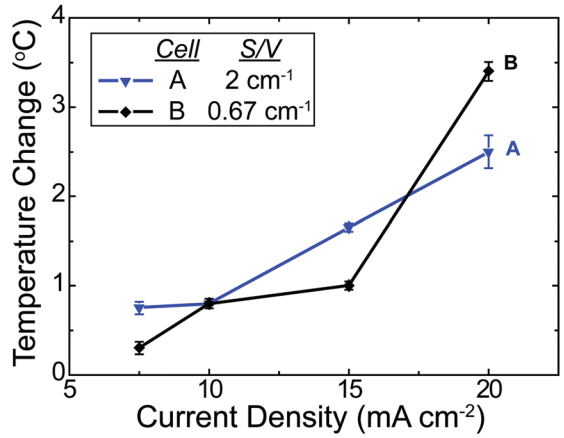

Fig. 4 *In situ* electrolyte heating experiments: the two electrochemical cells, A and B, with the same electrode surface areas and different electrolyte volumes (giving different *S/V* ratios), were operated under CO2R conditions with a Cu foil cathode in 0.1 M $NaHCO_3$ buffer. The temperature rise in the cell was monitored until a steady-state value was obtained. At current densities up to 15 mA cm^{-2} both cells maintain temperature changes less than 2 °C and even at the maximum current density of 20 mA cm^{-2} the temperature change was less than 4 °C. From the equilibrium calculations discussed in the text, the dissolved CO_2 concentration will change by less than 10% in both cells.

and less than 4 °C for a current density of 20 mA cm^{-2}. It was initially surprising that cell B, which has a larger thermal mass due to the larger electrolyte volume, showed a larger temperature change at high current densities. However, we note that the distance between the anode and cathode is larger for cell B: 25.5 mm *vs.* 11.5 mm for cell A. We infer that at higher current densities, the greater distance between the two working electrodes, and the increased resistive heating, leads to the larger temperature rise.

Hori and co-workers have studied the effects of temperature on the product distribution of CO2R on Cu foil, finding that increasing the electrolyte temperature caused an increase in selectivity towards hydrogen and ethylene and a decrease in selectivity towards methane in 0.5 M $KHCO_3$.[10] However, for the cells evaluated here, the change in electrolyte temperature is not large enough to have a considerable impact on product distribution according to those results. For instance, in Hori's work on Cu foil, a change from 10 °C to 20 °C changed the methane production by less than 10% faradaic efficiency. Moreover the concerns of temperature increase could be mitigated with improved external temperature controls, like air circulation or a water bath, as has been applied in previous CO2R studies[10,14] and other areas of electrochemical research.[39]

Effect of CO_2 supply to the electrochemical cell

The CO_2 concentration in the electrolyte can be experimentally measured by a measurement of the pH and temperature, as shown in Fig. 2. For example, a 0.1 change in pH corresponds to a ~25% change in the dissolved CO_2 concentration. A typical pH probe is capable of measuring with an accuracy of 0.01 pH units. Near the equilibrium pH of 6.83, this results in an uncertainty of only ~2% in the measurement of the dissolved CO_2 concentration using this method.

To assess CO_2 depletion in the electrochemical cells, the electrolyte pH was monitored before and after 1 hour of electrolysis as a function of current density as shown in Fig. 5. The shading denotes the border between the super-saturated regime (pH < 6.82) and under-saturated regimes, relative to the equilibrium value at 25 °C and 1 atm of CO_2. For all the experimental conditions tested in both cells, the electrolyte pH increased from the initial super-saturated value of ~6.7. In cell A, the electrolyte became under-saturated for current densities greater than 7.5 mA cm^{-2}, with a pH increase as large as 0.35 pH units at 20 mA cm^{-2}. In contrast, in cell B the increases in pH were smaller, less than 0.1 pH units, except at the highest current density where the electrolyte became slightly unsaturated.

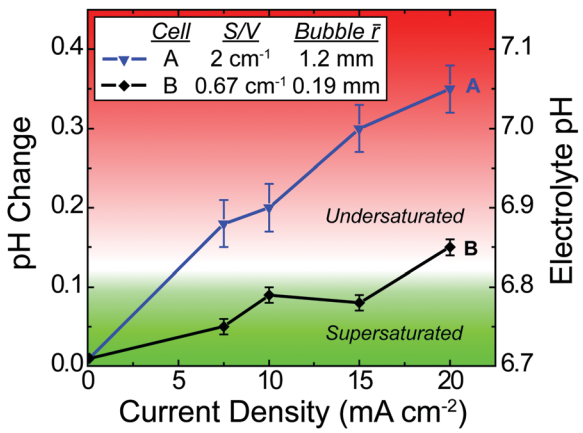

Fig. 5 *In situ* dissolved CO_2 depletion experiments: the two electrochemical cells, A and B, with different size CO_2 sparging bubbles were operated under CO2R conditions with a Cu foil cathode in 0.1 M $NaHCO_3$ buffer. The electrolyte pH change was measured after 1 hour of operation. It was found that the small bubbles (cell B, $\bar{r}$ = 0.19 mm) enabled the electrolyte to maintain CO_2 saturation up to 15 mA cm^{-2} whereas the larger CO_2 bubbles were unable to do so (cell A, $\bar{r}$ = 1.2 mm) at any current density.

The pH changes are much larger than any which would be expected due to temperature rise in the cell. Even at the maximum temperature rise observed above (4 °C), the change in pH would be less than 0.03 pH units. Thus, the increase in pH is due to a decrease in CO_2 concentration, which can be quantified using the relationships shown in Fig. 2. For example, at 10 mA cm^{-2} the steady state CO_2 concentration in cell A was ~63% of the initial value, whereas in cell B the CO_2 concentration was higher, ~82% of the initial concentration.

Cells A and B are identical in design except for their S/V and bubble introduction method. In cell A (S/V 2 cm^{-1}) a capillary tube was used to introduce CO_2 into the cell. In cell B (S/V 0.67 cm^{-1}) a glass P4 frit was used to introduce CO_2 into the cell (see Experimental for how bubbler was chosen). It is expected that smaller bubbles will improve gas to liquid CO_2 mass transfer and thus prevent CO_2 depletion. Still frame imaging was used to capture pictures of the bubbles in the cells and statistical analysis was performed to obtain an average spherical bubble size (Fig. 6 and Fig. S6, ESI†). The capillary bubbler produced 1.2 ± 0.07 mm radius bubbles and the glass frit produced 0.19 ± 0.05 mm radius bubbles. Clearly the smaller bubble size aided in maintaining the concentration of CO_2 in the electrolyte, although it had no effect on the starting point.

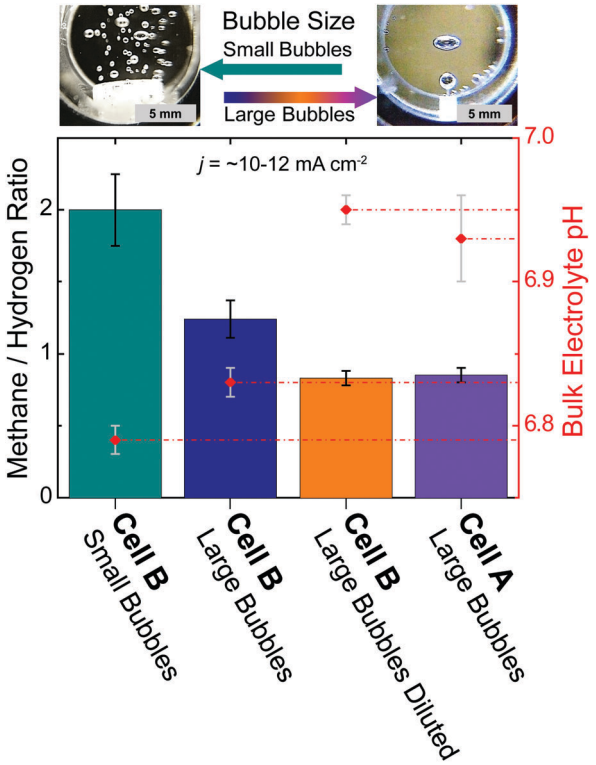

Fig. 6 The effect of CO_2 depletion on CO2R product distribution: CO2R experiments were performed in 0.1 M $NaHCO_3$ with Cu foil held at −1.05 V *vs.* RHE with various CO_2 feed conditions. The methane to hydrogen faradaic efficiency ratio is reported as well as the bulk electrolyte pH observed after 1 hour of operation. (B: small bubbles) cell B with a P4 frit bubbler, (B: large bubbles) cell B with a capillary tube bubbler, (B: large bubbles diluted) cell B with a capillary tube bubbler, bubbled with 75% CO_2 25% Ar, (A: large bubbles) cell A with a capillary tube bubbler. Methane is the dominant and expected product from Cu foil at this potential; however, if the CO_2 concentration decreases due to poor gas–liquid mass transfer, hydrogen becomes the dominant product. The observed current was ~10–12 mA cm^{-2} for all conditions tested.

The effect of CO_2 depletion in the electrolyte was further explored by examining the product distribution. Experiments were performed at −1.05 V *vs.* RHE (current density ~10–12 mA cm^{-2} for all experiments) and the ratio of methane to hydrogen faradaic efficiency was used as a figure of merit, as shown in Fig. 6. In cell B, which had small bubbles produced by the frit and a steady-state CO_2 concentration which was ~80% of the initial concentration, a CH_4/H_2 ratio of 2 was observed. In cell A, which had a steady state CO_2 concentration only ~60% of the initial value, the CH_4/H_2 was less than 1, which is significantly smaller than in cell B with the smaller bubbles.

To verify the crucial role of the bubble size, and hence the CO_2 mass transfer, the P4 frit bubbler in cell B was replaced with a capillary tube bubbler, which produces larger bubbles. Under the same Cu CO2R conditions, a shift in bulk electrolyte pH from 6.79 to 6.83 was observed, corresponding to a further 10% decrease in CO_2 concentration. Additionally, the methane to hydrogen ratio decreased (Fig. 6, cell B: large bubbles). While we would expect larger bubbles to lead to an increase in pH in both cells, it is not expected for this change to be exactly the same because of differences in the hydrodynamics in the two cells. Thus it was observed that the large bubbles lead to a smaller degree of CO_2 depletion in cell B than was observed in cell A. To further increase the CO_2 depletion in cell B, the CO_2 flow was diluted to 75% by volume with argon gas. Under this reaction condition the same (low) methane to hydrogen ratio was produced as seen in cell A (Fig. 6, cell B: large bubbles diluted). Moreover, the pH shift in cell B observed under this bubbling condition was almost identical to the pH shift seen in cell A, indicating that similar degrees of CO_2 depletion were produced. Based on these experiments, we conclude that the CO_2 depletion in the electrolyte causes the decrease in the methane to hydrogen ratio. Consistent with this conclusion, previous studies with copper electrodes have shown that reducing the CO_2 concentration by decreasing its partial pressure causes the methane to hydrogen ratio to decrease.[66]

It is expected that as the CO_2 concentration in the bulk electrolyte decreases, the corresponding concentration of CO_2 at the surface of the catalyst decreases.[33,67,68] We evaluated this effect by adapting the simple 1D diffusion model of Gupta *et al.*[69] to calculate the surface concentration of CO_2 and the pH (details in ESI†). The model predicts a ~20% lower CO_2 concentration at the surface of the Cu catalyst in cell A compared to cell B and also a slight decrease in pH (Fig. S8 and Tables S6 and S7, ESI†). The decrease in CO_2 concentration at the electrode would favor hydrogen evolution over CO_2 reduction, which is what is experimentally observed. We note that this change in product distribution could have been incorrectly attributed to catalyst deactivation, a common concern with CO2R catalysts,[25] instead of being the result of inadequate gas–liquid mass-transfer in the cell. Additional details, including faradaic efficiency data for all observed products, are given in the ESI.†

Implications of mass transfer for CO2R reactor design

Gas–liquid mass transfer and its effect on the properties of electrochemical cells have been widely studied.[42,45] The extensive literature on gas–liquid mass transfer for bubble column reactors[70–79] can be used to develop insights into how CO_2 mass transfer from the electrolyte to the cathode can be improved in high S/V cells.

The steady state mass balance for CO_2 dissolution into the electrolyte and its consumption at the cathode is given by:

$$N_{CO_2} S_c V^{-1} = K_L a (c^* - c^b), \quad (6)$$

where N_{CO_2} is the flux of CO_2 consumed at the electrode surface, S_c is the surface area of the catalyst, V is the electrolyte volume, K_L is the liquid mass transfer coefficient in the two-phase system, a is the interfacial surface area of the bubbles per volume of liquid, c^* is the solubility limit of carbon dioxide in water, and c^b is the concentration of carbon dioxide in the electrolyte. As demonstrated by the experiments presented above, it is desirable to keep c^b as close to c^* as possible. Thus, for a given total consumption rate of CO_2 (the product of N_{CO_2} and S_c), large values of $K_L a$ are required.

Since it is difficult to decouple K_L and a, they are frequently treated as a single variable.[71,75–78] $K_L a$ has been shown to be a function of the gas and liquid composition used, the characteristic size of the reactor, and the gaseous volume fraction (also known as the gas hold up).[71,75,76,78] The gaseous volume fraction is directly related to the superficial velocity of the gas.[71,73,80] Of the above mentioned parameters, the superficial gas velocity has the strongest effect on $K_L a$.[73,75,80] Thus for the following discussion, ways to modulate the superficial velocity will be the focus. To maintain a 0.1 mM decrease of c^b from c^*, a $K_L a$ of greater than $\sim 10^{-2}$ s^{-1} is necessary in our cell, for typical CO_2 surface fluxes. This should be accessible within a reasonable range of superficial gas velocities, based on previous measurements for bubble column reactors.[80]

The superficial velocity is defined as

$$U_s = Q/A_x, \quad (7)$$

where U_s is the superficial velocity, Q is the volumetric gaseous flow rate, and A_x is the cross sectional area for gas flow. Thus U_s can be increased by increasing Q or decreasing A_x. From an experimental perspective, Q is the easiest variable to control; however, the value of Q must be kept below a level at which entrainment of electrolyte will occur, resulting in electrolyte loss from the cell. While A_x can be designed to be smaller, for a fixed value of S/V, a decrease in A_x requires an increase in the height of the electrolyte column. Increasing the cell height might be expected to lead to bubble coalescence and a corresponding decrease in $K_L a$;[81] however, this effect is unlikely to be significant due to the short height of typical electrochemical cells.

It is also possible to increase the gas hold up by decreasing the bubble size, the effect that was exploited here. The gas hold up increases with decreasing bubble size for a given superficial velocity, because smaller bubbles rise more slowly than larger bubbles.[81,82] The lower rise time of smaller bubbles reduces the value of K_L; however, the larger increase in a overcomes this effect, leading to an overall increase in $K_L a$ for small bubbles.[81] Changing the bubble size in the cell can be accomplished by changing the gas inlet into the cell, but precise control over the bubble size requires further investigation, as it depends on the flow rate of gas, interfacial surface tension, and hydrophobicity of the gas inlet material.[71] Here, the optimal engineering solutions available to us were implemented to create a high S/V cell with a small bubble size (see ESI† for schematic drawings). However, further increases in S/V would be possible if smaller frit bubblers or some other small bubble sparging device could be implemented.

As the rate of CO_2 consumption at the cathode increases, the magnitude of $K_L a$ needed to maintain electrolyte saturation increases. For example, an electrode would consume $\sim$10 nMol of CO_2 cm^{-2} s^{-1} if it produces 100% CO operating at 2 mA cm^{-2} or 100% CH_4 operating at 8 mA cm^{-2}. Thus it is clear that if a CO2R experiment is conducted at high current density, the conditions for mass transfer and thus $K_L a$ are more stringent. An alternative way to conduct these experiments is in a liquid flow cell where the liquid is saturated with CO_2 externally and the pH of the effluent from the cell is actively monitored to ensure CO_2 saturation conditions are maintained. The disadvantage of using electrolyte recirculation is that it would most likely require a larger volume of electrolyte, thereby lengthening the time required to accumulate a sufficient concentration of liquid-phase products to be detectable. This issue has been considered recently in more detail by Clark *et al.*[35]

Conclusions

Electrochemical CO_2 reduction on Cu foil, performed in two small cells with similar design, illustrates the importance of maintaining cell electrolyte temperature and dissolved CO_2 saturation in order to perform rigorous CO2R catalyst characterization. While in this study, heating was not found to be a major concern at typically employed current densities, it is nevertheless recommended to measure electrolyte temperature in all cell designs.

In contrast, depletion of CO_2 in the bulk was found to be a larger effect, particularly in the cell with small electrolyte volume and thus a high S/V ratio (cell A). In the larger cell (cell B), CO_2 depletion was mitigated by using a glass frit bubbler which produces small bubbles, less than 0.2 mm in radius. The improved mass transfer of these smaller bubbles maintained the CO_2 concentration at a steady-state near equilibrium condition throughout the reduction experiments, as monitored by pH. In contrast, use of a capillary tube in the same cell, producing larger bubbles, caused depletion of CO_2. Most importantly, the CO_2 depletion caused large changes in the relative faradaic efficiencies of CO2R experiments on Cu foil: a decrease from 65% to 45% FE to CH_4 and an increase of 33% to 54% FE for H_2. We note that these changes could have been incorrectly interpreted as a decrease in catalyst selectivity or as catalysts deactivation. Thus we recommend that pH be actively monitored

to ensure near-equilibrium conditions are maintained over the course of the reaction, particularly in small volume cells. We note that it would be interesting to explore the effects of CO_2 pressure on mass transfer in a future study as our present cell design does not allow these types of studies.

Guidance from existing gas–liquid mass transfer models is used to understand how to meet the mass transfer requirements of the CO2R reaction. Finally, we provide the design parameters for a small volume, high S/V ratio, electrochemical cell for CO_2 reduction over Cu that can be operated at current densities of up to 15 mA cm^{-2} with a minimal temperature change of 2 °C while maintaining the electrolyte at near equilibrium saturation (CAD drawings available in ESI†).

Acknowledgements

Initial fabrication and cell design testing were supported by the California Energy Commission under agreement 500-11-023. Detailed CO2R testing and modelling of the electrochemical cell were performed within the Joint Center for Artificial Photosynthesis, a DOE Energy Innovation Hub, supported through the Office of Science of the U.S. Department of Energy under Award Number DE-SC0004993. EC acknowledges support from the National Science Foundation Graduate Fellowship. We thank Eric Granlund, the manager of the Berkeley College of Chemistry Machine Shop, for his expertise in machining and cell fabrication and Yanwei Lum for helpful discussions. We thank Adams and Chittenden Scientific Glass for their assistance in designing the frit unit.

References

1 K. Hashimoto, H. Habazaki, M. Yamasaki, S. Meguro, T. Sasaki, H. Katagiri, T. Matsui, K. Fujimura, K. Izumiya, N. Kumagai and E. Akiyama, *Mater. Sci. Eng., A*, 2001, **304–306**, 88–96.
2 C. Graves, S. D. Ebbesen, M. Mogensen and K. S. Lackner, *Renewable Sustainable Energy Rev.*, 2011, **15**, 1–23.
3 G. Centi and S. Perathoner, *Green Carbon Dioxide*, John Wiley & Sons, Inc., Hoboken, NJ, USA, 2014, pp. 1–24.
4 G. Centi, S. Perathoner, G. Wine and M. Gangeri, *Green Chem.*, 2007, **9**, 671–678.
5 M. Gattrell, N. Gupta and A. Co, *Energy Convers. Manage.*, 2007, **48**, 1255–1265.
6 J. Newman, P. G. Hoertz, C. A. Bonino and J. A. Trainham, *J. Electrochem. Soc.*, 2012, **159**, A1722–A1729.
7 A. Goeppert, M. Czaun, J.-P. Jones, G. K. Surya Prakash and G. A. Olah, *Chem. Soc. Rev.*, 2014, **43**, 7995–8048.
8 T. E. Teeter and P. Van Rysselberghe, *J. Chem. Phys.*, 1954, **22**, 759–760.
9 Y. Hori, K. Kikuchi and S. Suzuki, *Chem. Lett.*, 1985, 1695–1698.
10 Y. Hori, K. Kikuchi, A. Murata and S. Suzuki, *Chem. Lett.*, 1986, 897–898.
11 Y. Hori, A. Murata, R. Takahashi and S. Suzuki, *Chem. Lett.*, 1987, 1665–1668.
12 Y. Hori, A. Murata, R. Takahashi and S. Suzuki, *J. Am. Chem. Soc.*, 1987, **109**, 5022–5023.
13 Y. Hori, A. Murata and R. Takahashi, *J. Chem. Soc., Faraday Trans. 1*, 1989, **85**, 2309–2326.
14 Y. Hori, *Modern Aspects of Electrochemistry*, Springer New York, New York, NY, 2008, vol. 29, pp. 89–189.
15 Q. Lu, J. Rosen, Y. Zhou, G. S. Hutchings, Y. C. Kimmel, J. G. Chen and F. Jiao, *Nat. Commun.*, 2014, **5**, 3242.
16 M. Fan, Z. Bai, Q. Zhang, C. Ma, X.-D. Zhou and J. Qiao, *RSC Adv.*, 2014, **4**, 44583–44591.
17 F. S. Roberts, K. P. Kuhl and A. Nilsson, *Angew. Chem., Int. Ed.*, 2015, **54**, 5179–5182.
18 C. W. Li, J. Ciston and M. W. Kanan, *Nature*, 2014, **508**, 504–507.
19 M. Gattrell, N. Gupta and a. Co, *J. Electroanal. Chem.*, 2006, **594**, 1–19.
20 B. Kumar, M. Llorente, J. Froehlich, T. Dang, A. Sathrum and C. P. Kubiak, *Annu. Rev. Phys. Chem.*, 2012, **63**, 541–569.
21 J. Qiao, Y. Liu, F. Hong and J. Zhang, *Chem. Soc. Rev.*, 2014, **43**, 631–675.
22 Q. Lu, J. Rosen and F. Jiao, *ChemCatChem*, 2015, **7**, 38–47.
23 J. Albo, M. Alvarez-Guerra, P. Castaño and A. Irabien, *Green Chem.*, 2015, **17**, 2304–2324.
24 Z. Chen, T. F. Jaramillo, T. G. Deutsch, A. Kleiman-Shwarsctein, A. J. Forman, N. Gaillard, R. Garland, K. Takanabe, C. Heske, M. Sunkara, E. W. McFarland, K. Domen, E. L. Miller, J. A. Turner and H. N. Dinh, *J. Mater. Res.*, 2010, **25**, 3–16.
25 Y. Hori, H. Konishi, T. Futamura, a. Murata, O. Koga, H. Sakurai and K. Oguma, *Electrochim. Acta*, 2005, **50**, 5354–5369.
26 Y. Hori, A. Murata, R. Takahashi and S. Suzuki, *J. Chem. Soc., Chem. Commun.*, 1988, **109**, 17–19.
27 M. R. Singh, E. L. Clark and A. T. Bell, *Phys. Chem. Chem. Phys.*, 2015, **17**, 18924–18936.
28 C. W. Li and M. W. Kanan, *J. Am. Chem. Soc.*, 2012, **134**, 7231–7234.
29 K. Manthiram, B. J. Beberwyck and A. P. Alivisatos, *J. Am. Chem. Soc.*, 2014, **136**, 13319–13325.
30 D. Kim, J. Resasco, Y. Yu, A. M. Asiri and P. Yang, *Nat. Commun.*, 2014, **5**, 4948.
31 K. P. Kuhl, E. R. Cave, D. N. Abram and T. F. Jaramillo, *Energy Environ. Sci.*, 2012, **5**, 7050–7059.
32 S. Sen, D. Liu and G. T. R. Palmore, *ACS Catal.*, 2014, **4**, 3091–3095.
33 R. Kas, R. Kortlever, H. Yılmaz, M. T. M. Koper and G. Mul, *ChemElectroChem*, 2015, **2**, 354–358.
34 R. Kortlever, I. Peters, S. Koper and M. T. M. Koper, *ACS Catal.*, 2015, **5**, 3916–3923.
35 E. L. Clark, M. R. Singh, Y. Kwon and A. T. Bell, *Anal. Chem.*, 2015, **87**, 8013–8020.
36 B. A. Rosen, A. Salehi-Khojin, M. R. Thorson, W. Zhu, D. T. Whipple, P. J. A. Kenis and R. I. Masel, *Science*, 2011, **334**, 643–644.
37 H. Li and C. Oloman, *J. Appl. Electrochem.*, 2005, **35**, 955–965.
38 H. Hashiba, S. Yotsuhashi, M. Deguchi and Y. Yamada, *ACS Comb. Sci.*, 2016, **18**, 203–208.

39 R. W. Houghton and A. T. Kuhn, *J. Appl. Electrochem.*, 1974, **4**, 173–190.
40 R. E. W. Jansson, *Chem. Eng. Sci.*, 1980, **35**, 1979–2004.
41 D. R. Gabe and F. C. Walsh, *J. Appl. Electrochem.*, 1983, **13**, 3–21.
42 L. Sigrist, O. Dossenbach and N. Ibl, *Int. J. Heat Mass Transfer*, 1979, **22**, 1393–1399.
43 D. J. Economou, *J. Electrochem. Soc.*, 1985, **132**, 601.
44 O. N. Cavatorta and U. Bohm, *J. Appl. Electrochem.*, 1987, **17**, 340–346.
45 J. Reisener, M. A. Reuter and J. Krüger, *Chem. Eng. Sci.*, 1993, **48**, 1089–1101.
46 J. Newman and K. E. Thomas-Alyea, *Electrochemical Systems*, John Wiley & Sons, Inc., Hoboken, NJ, USA, 2004.
47 H. Zhong, K. Fujii, Y. Nakano and F. Jin, *J. Phys. Chem. C*, 2015, **119**, 55–61.
48 Y. Lum, Y. Kwon, P. Lobaccaro, L. Chen, E. L. Clark, A. T. Bell and J. W. Ager, *ACS Catal.*, 2016, **6**, 202–209.
49 J. Hong, W. Zhang, J. Ren and R. Xu, *Anal. Methods*, 2013, **5**, 1086–1097.
50 H. S. Harned and S. R. Scholes, *J. Am. Chem. Soc.*, 1941, **63**, 1706–1709.
51 H. S. Harned and R. Davis, *J. Am. Chem. Soc.*, 1943, **65**, 2030–2037.
52 J. J. Carroll, J. D. Slupsky and A. E. Mather, *J. Phys. Chem. Ref. Data*, 1991, **20**, 1201–1209.
53 A. V. Bandura and S. N. Lvov, *J. Phys. Chem. Ref. Data*, 2006, **35**, 15–30.
54 A. E. Markham and K. A. Kobe, *J. Am. Chem. Soc.*, 1941, **63**, 449–454.
55 R. F. Weiss, *Mar. Chem.*, 1974, **2**, 203–215.
56 A. Dickson and J. Riley, *Mar. Chem.*, 1979, **7**, 89–99.
57 F. J. Millero, D. Pierrot, K. Lee, R. Wanninkhof, R. A. Feely, C. L. Sabine, R. M. Key and T. Takahashi, *Deep Sea Res., Part I*, 2002, **49**, 1705–1723.
58 F. J. Millero, *Chem. Rev.*, 2007, **107**, 308–341.
59 U. Riebesell, V. J. Fabry, L. Hansson and J.-P. Gattuso, *Guide to best practices for ocean acidification research and data reporting*, Publications Office of the European Union Luxembourg, 2010.
60 J. Elhajj, M. Al-Hindi and F. Azizi, *Ind. Eng. Chem. Res.*, 2014, **53**, 2–22.
61 A. Schumpe, *Chem. Eng. Sci.*, 1993, **48**, 153–158.
62 S. Weisenberger and A. Schumpe, *AIChE J.*, 1996, **42**, 298–300.
63 L. N. Plummer and E. Busenberg, *Geochim. Cosmochim. Acta*, 1982, **46**, 1011–1040.
64 H. Hikita and Y. Konishi, *AIChE J.*, 1984, **30**, 945–951.
65 J. T. Kraemer and D. M. Bagley, *Biotechnol. Lett.*, 2006, **28**, 1485–1491.
66 G. Kyriacou and A. Anagnostopoulos, *J. Electroanal. Chem.*, 1992, **322**, 233–246.
67 R. Kas, R. Kortlever, A. Milbrat, M. T. M. Koper, G. Mul and J. Baltrusaitis, *Phys. Chem. Chem. Phys.*, 2014, **16**, 12194.
68 A. S. Varela, M. Kroschel, T. Reier and P. Strasser, *Catal. Today*, 2016, **260**, 8–13.
69 N. Gupta, M. Gattrell and B. MacDougall, *J. Appl. Electrochem.*, 2006, **36**, 161–172.
70 P. H. Calderbank and M. B. Moo-Young, *Chem. Eng. Sci.*, 1961, **16**, 39–54.
71 K. Akita and F. Yoshida, *Ind. Eng. Chem. Process Des. Dev.*, 1973, **12**, 76–80.
72 K. Akita and F. Yoshida, *Ind. Eng. Chem. Process Des. Dev.*, 1974, **13**, 84–91.
73 Y. T. Shah, B. G. Kelkar, S. P. Godbole and W.-D. Deckwer, *AIChE J.*, 1982, **28**, 353–379.
74 Y. Kawase and M. Moo-Young, *Can. J. Chem. Eng.*, 1992, **70**, 48–54.
75 W.-D. Deckwer and A. Schumpe, *Chem. Eng. Sci.*, 1993, **48**, 889–911.
76 K. Shimizu, S. Takada, K. Minekawa and Y. Kawase, *Chem. Eng. J.*, 2000, **78**, 21–28.
77 H. Dhaouadi, S. Poncin, J. M. Hornut and N. Midoux, *Chem. Eng. Process.*, 2008, **47**, 548–556.
78 M. Ramezani, N. Mostoufi and M. R. Mehrnia, *Ind. Eng. Chem. Res.*, 2012, **51**, 5705–5714.
79 M. C. Gruber, S. Radl and J. G. Khinast, *Chem. Eng. Sci.*, 2015, **137**, 188–204.
80 F. Yoshida and K. Akita, *AIChE J.*, 1965, **11**, 9–13.
81 R. Lau, P. H. V. Lee and T. Chen, *Chem. Eng. Process.*, 2012, **62**, 18–25.
82 R. Clift, J. R. Grace and M. E. Weber, *Bubbles, Drop, and Particles*, 1978.